JOC The Journal of Organic Chemistry

Article

pubs.acs.org/joc

Can Baird's and Clar's Rules Combined Explain Triplet State Energies of Polycyclic Conjugated Hydrocarbons with Fused 4*n*π- and (4*n* + 2)π-Rings?

Rabia Ayub,[†] Ouissam El Bakouri,[‡] Kjell Jorner,[†] Miquel Solà,*[,‡] and Henrik Ottosson*[,†]

[†]Department of Chemistry—Ångström Laboratory, Uppsala University, Box 523, SE-751 20 Uppsala, Sweden

[‡]Institut de Química Computacional i Catàlisi (IQCC), Universitat de Girona, c/Maria Aurèlia Capmany 6, 17003 Girona, Catalonia, Spain

Supporting Information

ABSTRACT: Compounds that can be labeled as "aromatic chameleons" are π-conjugated compounds that are able to adjust their π-electron distributions so as to comply with the different rules of aromaticity in different electronic states. We used quantum chemical calculations to explore how the fusion of benzene rings onto aromatic chameleonic units represented by biphenylene, dibenzocyclooctatetraene, and dibenzo[*a*,*e*]pentalene modifies the first triplet excited states (T_1) of the compounds. Decreases in T_1 energies are observed when going from isomers with linear connectivity of the fused benzene rings to those with cis- or trans-bent connectivities. The T_1 energies decreased down to those of the parent (isolated) 4*n*π-electron units. Simultaneously, we observe an increased influence of triplet state aromaticity of the central 4*n* ring as given by Baird's rule and evidenced by geometric, magnetic, and electron density based aromaticity indices (HOMA, NICS-*XY*, ACID, and FLU). Because of an influence of triplet state aromaticity in the central 4*n*π-electron units, the most stabilized compounds retain the triplet excitation in Baird π-quartets or octets, enabling the outer benzene rings to adapt closed-shell singlet Clar π-sextet character. Interestingly, the T_1 energies go down as the total number of aromatic cycles within a molecule in the T_1 state increases.

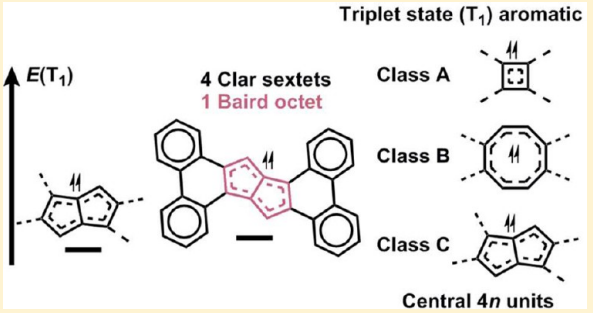

INTRODUCTION

π-Conjugated compounds comprised of fused (4*n* + 2)π- and 4*n*π-electron cycles, such as biphenylene and [N]phenylenes, are interesting for applications in organic and molecular electronics.[1−3] Yet, they are also of fundamental importance as their study sheds light on the limits of aromaticity and antiaromaticity and ultimately on chemical bonding.[4−8] In their electronic ground states (S_0), these compounds display properties that are intermediate between those of aromatic and antiaromatic systems, i.e., they display partial aromaticity.[9] However, how do these compounds behave in their first electronically excited states, and can their properties be understood in qualitative terms? Such qualitative understanding should facilitate the identification of new compounds with useful properties for applications.

Antiaromatic compounds generally have small HOMO−LUMO energy gaps ($\Delta\varepsilon_{HOMO-LUMO}$), low-lying triplet states, and lower excitation energies than aromatic ones.[10] The triplet state aromatic character of [4*n*]annulenes was first analyzed by Baird in 1972,[11] and he concluded that [4*n*]annulenes switch from being antiaromatic in S_0 to aromatic in their lowest ππ* excited triplet (T_1) states. The opposite applies for [4*n* + 2]annulenes, which become antiaromatic in their T_1 states.[12] Later it has been shown that [4*n*]annulenes are also aromatic in their lowest singlet excited (S_1) states.[13,14] We have earlier argued that Baird's rule can be used as a back-of-an-envelope tool for rationalization of the fundamental properties of various classes of π-conjugated molecules.[15] Indeed, we found that certain hydrocarbon compounds which we described as "aromatic chameleons" are able to adjust their electronic structure so as to comply with Hückel's 4*n* + 2 rule for aromaticity in the S_0 state and Baird's 4*n* rule for aromaticity in the T_1 and S_1 states.[15,16]

Fulvenes were identified as one class of aromatic chameleon compounds as they can be influenced by resonance structures in which the π-electron pair of the exocyclic C═C bond is pushed in or out of the ring (Figure 1A), allowing them to adjust the π-electron count in the ring from the Hückel-aromatic 4*n* + 2 to the Baird-aromatic 4*n*. Biphenylene could tentatively also be considered as an aromatic chameleon (Figure 1B) because in the S_0 state it can be influenced by a resonance structure with two 6π-electron benzene rings while in the T_1 state it can be described by four different Baird-aromatic resonance structures; one with a 12π-electron biradical perimeter (T_1-**I**), two equivalent ones with 8π-

Received: April 15, 2017
Published: May 23, 2017

DOI: 10.1021/acs.joc.7b00906
J. Org. Chem. 2017, 82, 6327−6340

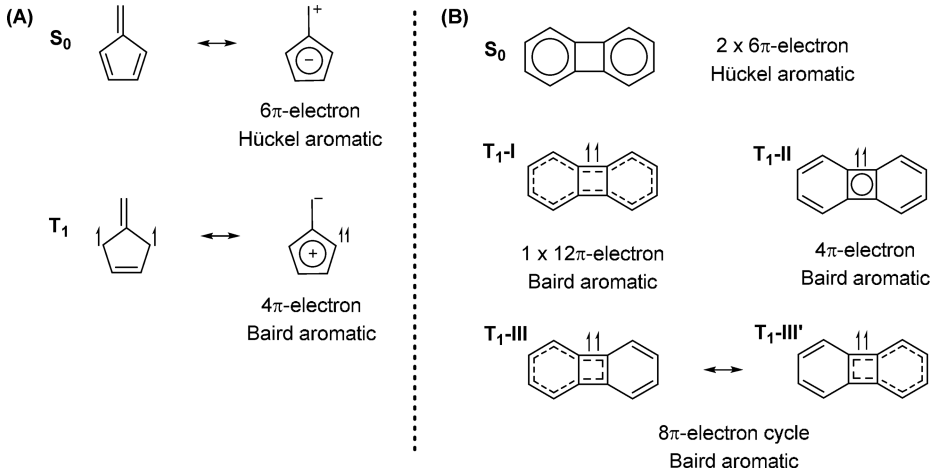

Figure 1. Aromatic resonance structures in the S_0 and T_1 states of (A) pentafulvene (polar) and (B) biphenylene (nonpolar) showing how they can act as an "aromatic chameleon" compounds.

electron circuits ($\mathbf{T_1}$-**III** and $\mathbf{T_1}$-**III**′), and one with a central 4π-electron cycle ($\mathbf{T_1}$-**II**). Yet, biphenylene in its S_0 state can also be labeled as a Hückel-antiaromatic, and previous computational studies indicated that biphenylene in this state has localized C−C bonding and some antiaromatic character in the 12π-electron perimeter.[17]

The identification of new molecular motifs possessing useful properties for organic electronics applications is a growing area of molecular design. Significant focus is placed on polycyclic aromatic hydrocarbons (PAHs), even though certain of these compounds are of low stability. Elongating linear acenes is one way to decrease the $\Delta\varepsilon_{\mathrm{HOMO-LUMO}}$, but it is challenging because already pentacene is reported to dimerize and to be oxidized at ambient conditions.[18] Pentacene and longer series of acenes can be stabilized through substitution[19,20] or through incorporation of heteroatoms or nonhexagonal carbocycles within the framework.[21,22] Another design strategy to compounds with low-lying excited states and interesting optical properties is to introduce (formally) antiaromatic 4$n\pi$-electron units such as the pentalene unit.[23] π-Conjugated dinaphthoindacene isomers and diphenanthroindacene analogues were synthesized recently and reported to show less negative redox potential as a consequence of increasing paratropicity of the antiaromatic central unit.[24] Hence these kinds of molecular scaffolds could be potential candidates for organic semiconductors.

We now investigated compounds with fused [4n + 2]- and [4n]-conjugated circuits but with overall 4$n\pi$-electron perimeters, and we test if the T_1 state properties can be rationalized by usage of Baird's rule combined with Clar's rule. When applied to a PAH, the latter rule tells that the resonance structure which has the largest number of disjoint aromatic π-sextets is more important than the resonance structures with a smaller number of Clar π-sextets.[25,26] Additionally, the isomer among a series of PAH isomers that can host the largest number of disjoint aromatic π-sextets (cf. benzene rings) is the thermodynamically most stable one. Previously, it has been reported that bent PAHs are more stable than their linear isomers in the S_0 state because they can host more Clar π-sextets, e.g., phenanthrene hosts two π-sextets when compared to one for anthracene.[27,28] Moreover, a linear correlation between the relative isomer energies (thermodynamic stability)[29] and excitation energies[30] with the number of Clar π-sextets was reported for a series of heptabenzenoid isomers. Clar's rule can also be extended to heterocyclic systems as it has been shown that Clar structures exist in boron nitride (BN) analogues of PAHs.[31]

If a compound has both (4n + 2)π- and 4$n\pi$-electron rings we hypothesize that the isomer with the lowest energy in the T_1 state is that isomer which allows for the largest number of aromatic rings, i.e., disjoint triplet diradical Baird-aromatic 4$n\pi$-electron rings (Baird π-quartets or π-octets) plus disjoint singlet closed-shell Hückel-aromatic π-sextet rings (Clar π-sextets). If Baird's rule can be used together with Clar's rule and influence the relative isomer energies in the T_1 state, then the different connectivity of various isomers should also have an impact on the T_1 state energies ($E(T_1)$). Thus, by regarding the triplet state aromaticity one could potentially rationalize the first excited state energies, something which is less straightforward based on the shapes of HOMO and LUMO and $\Delta\varepsilon_{\mathrm{HOMO-LUMO}}$. For this purpose, three central 4$n\pi$-electron cycles (cyclobutadiene (CBD), cyclooctatetraene (COT), and pentalene (PEN)) were considered (Figure 2), and we examine our working hypothesis that Clar's and Baird's rules can be used in combination. We particularly address the scope and limitations of the hypothesis, for which compounds does it work and for which ones not? Although the present study is fundamental in character it shows on a direction for rational tuning of the $E(T_1)$ and $\Delta\varepsilon_{\mathrm{HOMO-LUMO}}$ that should be useful for design of novel compounds for organic electronics.

COMPUTATIONAL METHODS

The Gaussian 09 program package, revision D.01, is applied for the bulk of the quantum chemical calculations.[32] The geometry optimizations were carried out at the B3LYP level[33] employing the 6-311G(d,p)[34] basis set. The harmonic vibrational analytical frequency calculations of the optimized structures showed no imaginary frequencies (N_{img} = 0), verifying real minima. The energies reported are zero-point corrected adiabatic electronic energies. The stability test of the wave function using the "stable" keyword in Gaussian 09 confirmed that the electronic ground states are closed-shell singlets and not open-shell singlets. For molecules with COT rings there are possibilities for several different conformers in their S_0 states. Only in one case (compound *trans*-**B3BB**) did we find two stable S_0 state conformers, and below we discuss the properties of the most stable of these.

The magnetic shielding properties in π-conjugated polycyclic compounds are analyzed by NICS-*XY*-scans and ACID plots. The

DOI: 10.1021/acs.joc.7b00906
J. Org. Chem. 2017, 82, 6327−6340

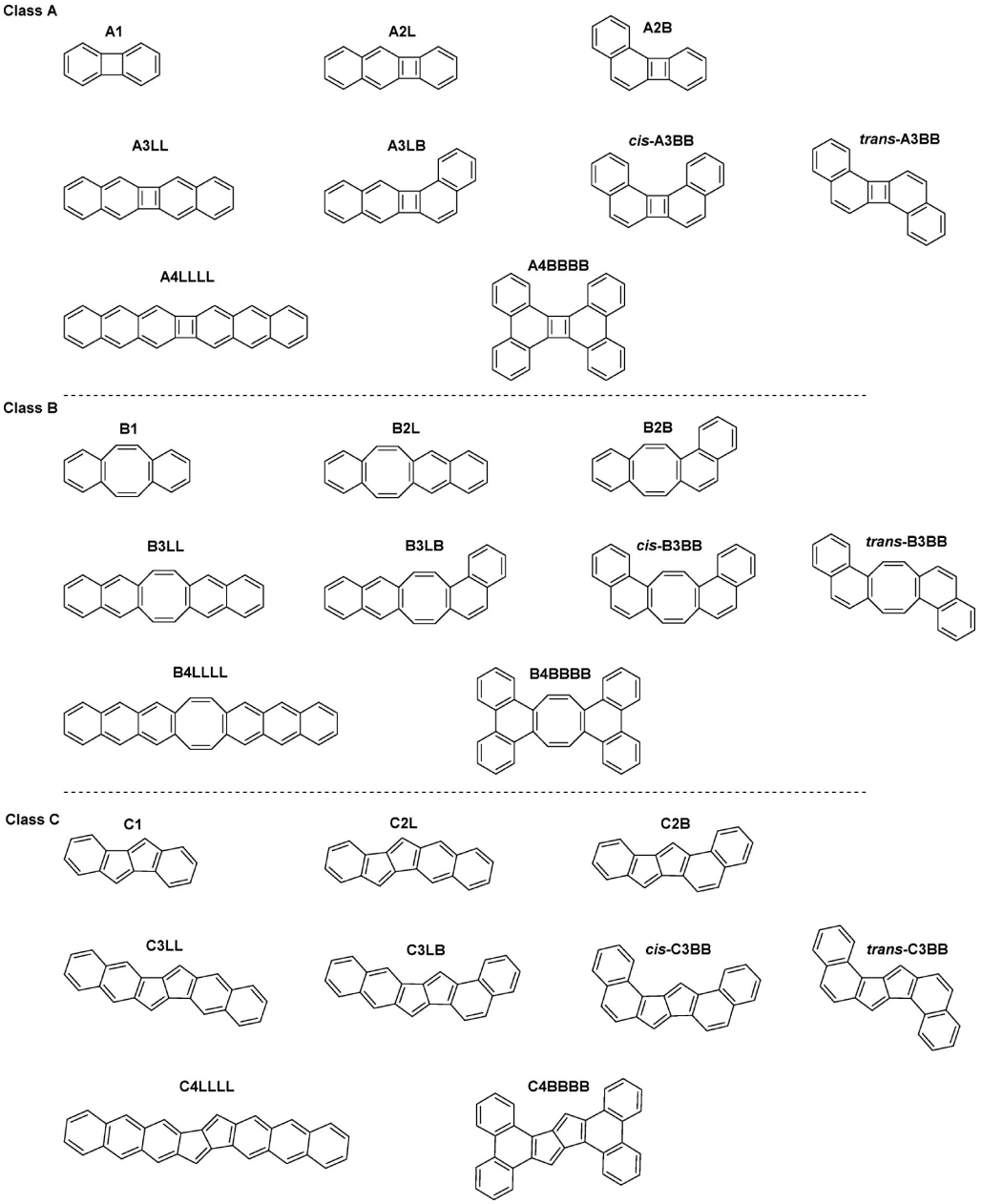

Figure 2. Classes of compounds studied: L, linear; B, bent.

NICS-*XY*-scans can distinguish the global (current along the perimeter of the whole molecule) and local (current inside each circuit) currents in π-conjugated polycyclics. The NICS-*XY*-scans are calculated at the GIAO-(U)B3LYP/6-311+G(d,p) computational level and performed with the Aroma package (1.0) of Stanger and co-workers using cphf = grid = fine and integral = grid = ultrafine keywords.[35−39] The NICS-*XY*-scans were recorded at 1.7 Å above the molecular plane, as recommended by Stanger, and only contain π contributions by employing the σ-only model. A negative/positive NICS-*XY*-scan represents a global current due to the simultaneous presence of global, semiglobal, and local currents. The anisotropy of the induced current density (ACID) calculations[40] were used to analyze the ring-currents with the CGST method[41] at the (U)B3LYP/6-311+G(d,p) level. The ACID plots were generated using (NMR = CGST IOp(10/93 = 1) and ultrafine grid (integral = grid = ultrafine). The harmonic oscillator model of aromaticity (HOMA) was used as a structural index of aromaticity and values were calculated at the (U)B3LYP/6-311G(d,p) level.[42] The HOMA(peri) values based on the CC bonds of the perimeter of the whole molecules are also considered. Positives values close to one correspond to aromatic compounds, negative to antiaromatic compounds, and values close to zero correspond to nonaromatic compounds.

The aromatic fluctuation index (FLU)[43] was calculated at the B3LYP/6-311+G(d,p)//B3LYP/6-311G(d,p) level of theory and was computed using electron sharing indices (ESI)[44] with the expression:

$$\mathrm{FLU}(\mathcal{A}) = \frac{1}{N}\sum_{i=1}^{N}\left[\left(\frac{V(A_i)}{V(A_{i-1})}\right)^{\alpha}\left(\frac{\delta(A_i, A_{i-1}) - \delta_{\mathrm{ref}}(A_i, A_{i-1})}{\delta_{\mathrm{ref}}(A_i, A_{i-1})}\right)\right]^2 \quad (1)$$

where $A_0 \equiv A_N$ and the string $\mathcal{A} = \{A_1, A_2, ..., A_N\}$ contains the ordered elements according to the connectivity of the N atoms in a ring or in a chosen circuit (FLU can be calculated for any arbitrary circuit in a given molecule). $V(A)$ is defined as

$$V(A_i) = \sum_{A_j \neq A_i} \delta(A_i, A_j) \quad (2)$$

DOI: 10.1021/acs.joc.7b00906
J. Org. Chem. 2017, 82, 6327−6340

and α is a simple function to make sure that the first term is always greater or equal to 1, thus taking the values:

$$\alpha = \begin{cases} 1 & V(A_i) > V(A_{i-1}) \\ -1 & V(A_i) \leq V(A_{i-1}) \end{cases} \quad (3)$$

The delocalization index (DI) between atoms A and B, δ(A, B), is obtained by the double integration of the exchange-correlation density ($\gamma_{XC}(\vec{r}_1, \vec{r}_2)$) over the space occupied by atoms A and B:[45]

$$\delta(\mathrm{A}, \mathrm{B}) = -2 \int_{\mathrm{A}} \int_{\mathrm{B}} \gamma_{XC}(\vec{r}_1, \vec{r}_2)\, \mathrm{d}\vec{r}_1, \mathrm{d}\vec{r}_2 \quad (4)$$

For single-determinant wave functions (including density functional approaches), δ(A,B) is expressed as

$$\delta(\mathrm{A}, \mathrm{B}) = 2 \sum_{i,j}^{\mathrm{occ.MSO}} S_{ij}(\mathrm{A}) S_{ij}(\mathrm{B}) \quad (5)$$

The sums run over all the occupied molecular spin−orbitals (MSO). S_{ij}(A) is the overlap between MSOs i and j within the basin of atom A. We have made use of the Atoms-in-Molecules atomic partition defined from the condition of zero-flux gradient in the one-electron density $\rho(\mathbf{r})$ to compute $S_{ij}(A)$ values.[46] DI and FLU indices were obtained with the ESI-3D program[47] using the overlaps between occupied molecular orbitals in the atomic basins generated by the AIMAll program.[48] The $\delta_{ref}(C, C)$ reference value of 1.389 e used for C−C bonds in FLU calculations corresponds to the $\delta(C, C)$ of benzene computed at the B3LYP/6-311+G(d,p) level of theory. FLU is close to 0 in aromatic species and differs from it in nonaromatic ones. Finally, to analyze the Baird or Hückel-aromatic character of our systems in their triplet states, we split the FLU values into α and β contributions. Whereas identical or very similar values of FLU_α and FLU_β are expected in Hückel-aromatic species, significant differences ($\Delta FLU_{\alpha\beta} = FLU_\alpha - FLU_\beta \neq 0$) are anticipated in Baird-aromatic systems. As an indicator of Hückel (low values) or Baird (high values) aromatic character, we use the γ descriptor defined as the absolute value of the $\Delta FLU_{\alpha\beta}/FLU$ ratio. As defined, γ allows consistent comparisons between species with different absolute aromaticity FLU values. The γ descriptor was previously used for hybrid Hückel-Baird aromatic species with good results.[49] To compute FLU_α and FLU_β, the same eq 1 was used but now considering only the α or β MSOs and taking the $\delta_{ref}(C, C)$ reference value in eq 1 as half the reference value used for nonspin split FLU calculations.

RESULTS AND DISCUSSION

The three compound classes differ by the central unit being either a cyclobutadiene (CBD), cyclooctatetraene (COT), or

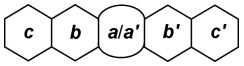

Figure 3. Labeling of different rings.

pentalene (PEN) moiety. The $E(T_1)$ and $\Delta\varepsilon_{HOMO-LUMO}$ of all compounds are reported at the (U)B3LYP/6-311G(d,p) level, and the influence of T_1 aromaticity is evaluated by the magnetic NICS and ACID indices, the electronic FLU index, and the geometric HOMA index. The rings in the various compounds are labeled so that the central 4$n\pi$-electron ring is always ring ***a*** or rings ***a*** and ***a***′ in the case of pentalene, as shown in Figure 3. In the case of symmetric compounds rings ***a***′, ***b***′, and ***c***′ are equivalent to rings ***a***, ***b***, and ***c***, respectively.

Potential Nonpolar "Aromatic Chameleon" Compounds. The central ring ***a*** in the class **A** compounds can be viewed as a 4π-electron CBD ring or alternatively as the four-membered ring in [4]radialene. The first compound in this series, biphenylene (**A1**),[17,50] was suggested above to have an "aromatic chameleon" feature (Figure 1).[12] Yet, is this labeling in accordance with computational results? For **A1** in the S_0 state (**A1**(S_0)) the NICS-*XY* profile in Figure 4A shows that the $NICS_{\pi zz}$ values are 9.5 ppm for the ***a*** ring and merely −7.6 ppm for the ***b*** rings (in the center of each ring), suggesting that the latter rings are weakly aromatic (the corresponding $NICS_{\pi zz}$ values for CBD and benzene in their S_0 states are 18.3 and −17.6 ppm, respectively, at the (U)B3LYP/6-311+G(d,p) level, given in Figure S9). The NICS-*XY*-scan of **A1**(S_0) is the same as the previously reported one.[36] The ACID plot of **A1**(S_0) (Figure S19) shows that ring ***a*** has a strong paramagnetic ring-current while the ***b*** rings are only weakly aromatic. However, the corresponding FLU values are 0.0441 and 0.0052 (Table 1), and with a near-zero value for the ***b*** rings this suggests a substantial aromaticity in these rings contrasting the findings from NICS and ACID. The FLU value along the perimeter (0.0147) indicates that the π-electron delocalization is not particularly efficient along this path and that the most effective π-delocalization is locally in the six-membered rings (6-MRs). Finally, the HOMA values for the ***a*** and ***b*** rings are −1.109 and 0.847 (Figure 5), corresponding to local antiaromaticity and aromaticity, respectively. The HOMA(peri) around the 12-atom perimeter is merely 0.271, supporting nonaromaticity. Taken together, all indices clarify that the antiaromaticity of the ***a*** ring in **A1**(S_0) is weaker than in the parent CBD while the aromaticity of the ***b*** rings is reduced somewhat when compared to that of benzene.

For **A1**(T_1), the NICS-*XY*-scan, and ACID plot (Figure 4) indicate that resonance structure $\mathbf{T_1}$**-I** (Figure 1) with a global diatropic ring-current is important. The $NICS_{(1.7)\pi zz}$ values of −15.4 and −10.2 ppm observed for the ***a*** and ***b*** rings, respectively, are also indicative of aromaticity. In the ACID plot for **A1**(T_1), the diamagnetic ring-current along the perimeter is apparent (Figure 4). The FLU values of the CBD and benzene rings are 0.0382 and 0.0169 (Table 1), respectively, revealing that when going from the S_0 to the T_1 state, the antiaromatic character of CBD decreases somewhat whereas the aromaticity of the 6-MR is significantly reduced. Because of its symmetry, **A1**(T_1) has four possible electronic circuits for 4$n\pi$-electron delocalization (Figure 1); one global along the perimeter ($FLU_{bab'}$ = 0.0082; for comparison, FLU in T_1 antiaromatic benzene is 0.0238), two semiglobal which involves the CBD ring and one benzene ring (FLU_{ab} = 0.0157), and one local corresponding to the CBD ring (FLU_a = 0.0382), respectively. The $FLU_{bab'}$ is the lowest, meaning that T_1 state π-electron delocalization occurs most efficiently along the perimeter. Moreover, the $\gamma_{bab'}$ value of 1.00 (Table 1) of the perimeter circuit indicates Baird-aromatic character, and consequently that resonance structure $\mathbf{T_1}$**-I** (Figure 1) best describes **A1**(T_1). Interestingly, the DIs explain why $FLU_{bab'}$ decreases and FLU_b increases significantly from the S_0 to the T_1 state. In short, the local circuit in the 6-MRs is blocked in the T_1 state, and the circuit through the perimeter is activated (see the Supporting Information for a more detailed analysis). Finally, the changes in aromaticity when going from the S_0 to the T_1 state are also apparent in the geometries. In the T_1 state, the HOMA(peri) value increases by 0.5 so that the perimeter of **A1**(T_1) can be described as an aromatic cycle. Simultaneously, the HOMA of the ***a*** ring (−0.401) is still representative of antiaromaticity. In this context, it should be noted that a previous study using HOMA found the parent cyclobutadiene in its T_1 state to be only weakly aromatic having a HOMA values of only 0.30.[51] Similar observations have been made in studies based on ELF_π

DOI: 10.1021/acs.joc.7b00906
J. Org. Chem. 2017, 82, 6327−6340

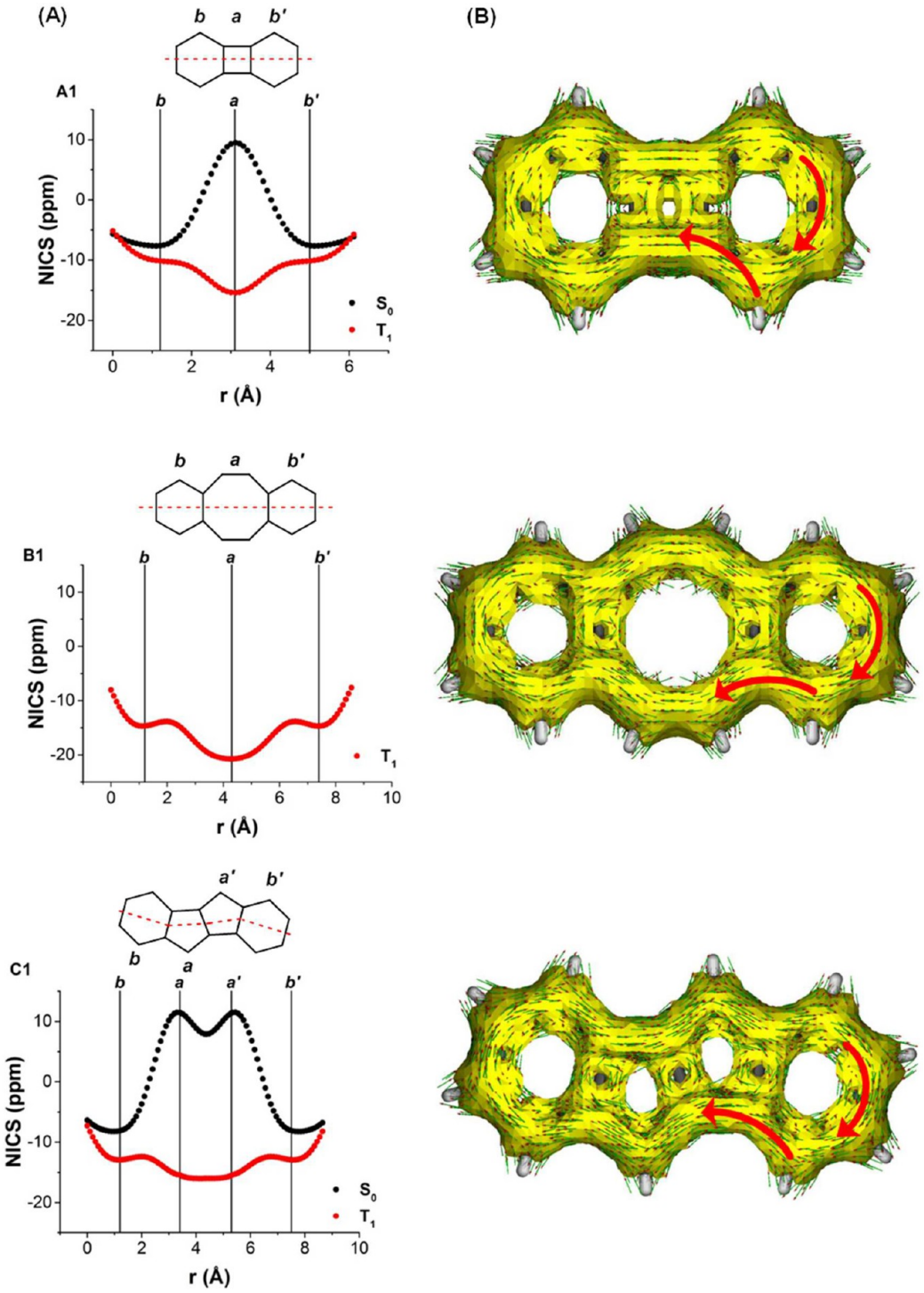

Figure 4. Calculated aromaticity indices for **A1**, **B1**, and **C1**. (A) NICS-*XY*-scans in the S_0 and T_1 states (for **B1** only the T_1 state) at the GIAO-(U)B3LYP/6-311+G(d,p)//(U)B3LYP/6-311+G(d,p) level and (B) ACID plots in the T_1 states (isosurface value, 0.045) at the (U)B3LYP/6-311+G(d,p) level.

as well as spin current density analysis.[52,53] The ISE value of CBD(T_1) is 0.8 kcal/mol higher than that of COT(T_1); however, Zhu and co-workers reported that the ISE values for small annulenes such as CBD are not reliable.[54]

So is **A1** an aromatic chameleon compound? It is certainly influenced by Hückel-aromaticity in its S_0 state, although different aromaticity indices give different results as to the extent of this influence. Moreover, it is influenced by Baird-aromaticity in the T_1 state. Accordingly, **A1** doubtlessly has an aromatic chameleon character. Yet, can this character be increased in dibenzofused compounds having central 8π-electron units instead of a 4π-electron unit?

The various aromaticity measures applied to **B1** and **C1** in their S_0 and T_1 states also reveal aromatic chameleon features. Compound **B1**(S_0) is nonplanar making NICS-*XY* not useful, and for this reason we instead carried out a NICS-scan perpendicular to one of the ***b*** rings,[39] revealing that these are strongly aromatic ($NICS_{(1.7)\pi zz}$ is −14.6 ppm, see Figure S10).

DOI: 10.1021/acs.joc.7b00906
J. Org. Chem. 2017, 82, 6327−6340

Table 1. FLU and γ_x Values Computed for All the Possible (Local, Semi-Global, and Global) Circuits in the S_0 and T_1 States for A1, B1, and C1

compound	electronic state	circuit along perimeter of ring(s)	FLU	γ_x
A1	S_0	*a*	0.0441	
		b	0.0052	
		a+*b*	0.0220	
		b+*a*+*b*′	0.0147	
	T_1	*a*	0.0382	0.3272
		b	0.0169	0.4140
		a+*b*	0.0157	0.5923
		b+*a*+*b*′	0.0082	1.0000
B1	S_0	*a*	0.0483	-
		b	0.0011	
		a + *b*	0.0323	
		b + *a* + *b*′	0.0243	
	T_1	*a*	0.0098	0.5816
		b	0.0150	0.0586
		a + *b*	0.0089	0.2228
		b + *a* + *b*′	0.0085	0.0118
C1	S_0	*a* + *a*′	0.0340	-
		b	0.0032	
		a + *a*′ + *b*′	0.0224	
		b + *a* + *a*′ + *b*′	0.0160	
	T_1	*a* + *a*′	0.0159	0.4865
		b	0.0131	0.5969
		a + *a*′ + *b*′	0.0097	0.5369
		b + *a* + *a*′ + *b*′	0.0066	0.6061

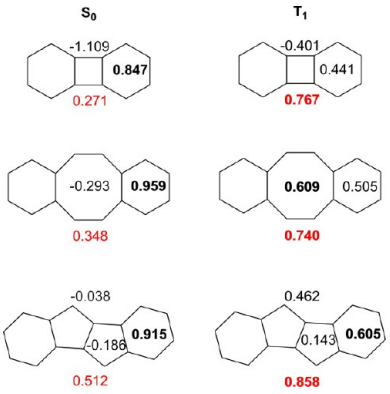

Figure 5. HOMA values for the S_0 and T_1 states at the (U)B3LYP/6-311G(d,p) level. The values in bold correspond to aromatic rings. The values in red indicate HOMA(peri).

Table 2. Relaxed Triplet State Energies $E(T_1)$ in eV at the (U)B3LYP/6-311G(d,p) Level

class A	$E(T_1)$	class B	$E(T_1)$	class C	$E(T_1)$
A1	1.92	**B1**	1.74	**C1**	1.33
A2L	2.22	**B2L**	2.40	**C2L**	1.42
A2B	1.42	**B2B**	1.67	**C2B**	1.02
A3LL	2.75	**B3LL**	2.04	**C3LL**	1.43
A3LB	1.68	**B3LB**	1.74	**C3BL**	1.14
cis-**A3BB**	1.06	*cis*-**B3BB**	1.61	*cis*-**C3BB**	0.79
trans-**A3BB**	1.03	*trans*-**B3BB**	1.69	*trans*-**C3BB**	0.78
A4LLLL	1.70	**B4LLLL**	1.61	**C4LLLL**	1.30
A4BBBB	0.62	**B4BBBB**	1.93	**C4BBBB**	0.58

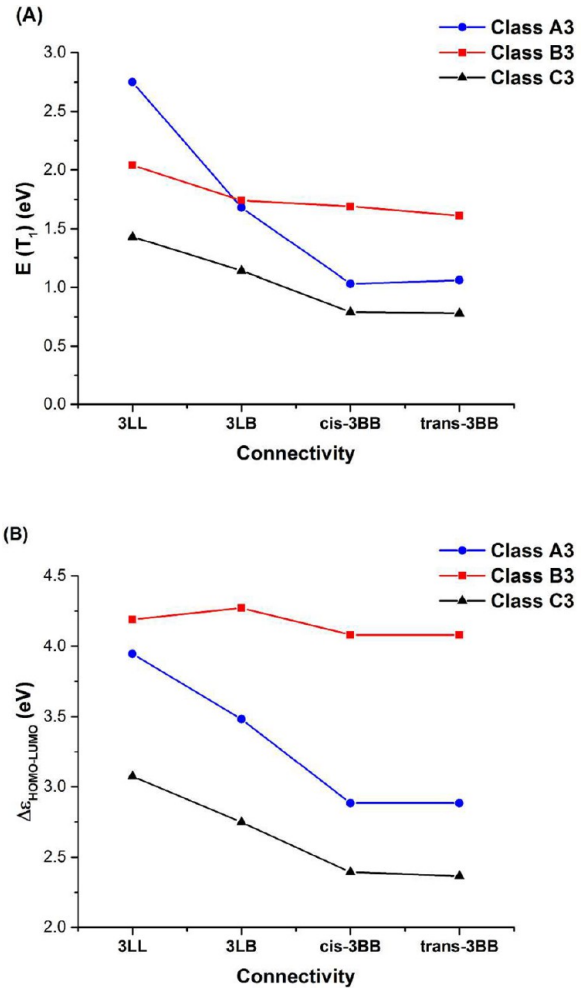

Figure 6. (A) $E(T_1)$ and (B) $\Delta\varepsilon_{HOMO-LUMO}$ as functions of the connectivity in the **A3**, **B3**, and **C3** classes of isomeric compounds.

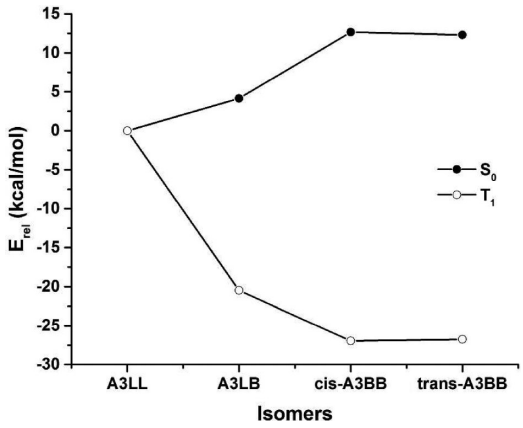

Figure 7. Relative energies E_{rel} (kcal/mol) of the **A3** isomers in the S_0 and T_1 states, respectively, with **A3LL** as the reference isomer in both states.

The ACID plot of **B1**(S_0) shows diamagnetic ring-currents in the outer benzene rings while the central ***a*** ring, the COT ring, is nonaromatic. In **C1**(S_0), the ***b*** and ***b***′ rings, and the central pentalene unit show local diatropic and paratropic ring-currents, respectively (Figure 4 and Figure S21). The FLU values for ring ***b*** of 0.0011 and 0.0032 (Table 1), respectively, show clear representation of two aromatic benzene rings in

DOI: 10.1021/acs.joc.7b00906
J. Org. Chem. 2017, 82, 6327−6340

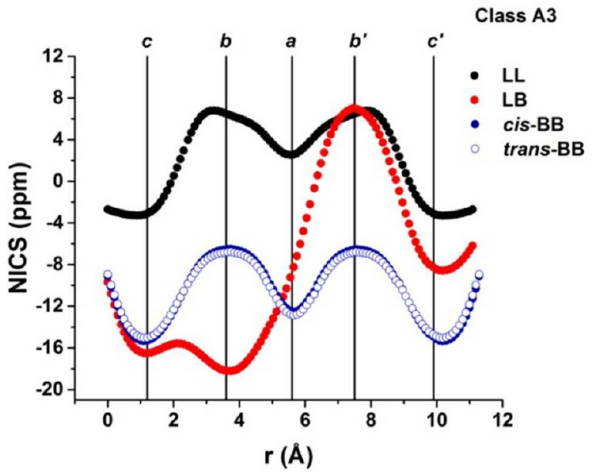

Figure 8. NICS-*XY*-scans at the UB3LYP/6-311+G(d,p) level of the four **A3** isomers in their T_1 states.

both **B1**(S_0) and **C1**(S_0), and this is also the description given by HOMA (Figure 5). With regard to the central ***a*** rings they are best described as nonaromatic according to FLU and HOMA. Finally, according to HOMA, the perimeter of **C1**(S_0) is weakly aromatic (HOMA(peri) = 0.512) while the perimeter of **B1**(S_0) is nonaromatic (HOMA(peri) = 0.348).

In the T_1 state, the NICS-*XY* profiles of **B1** and **C1** reveal diatropic ring-currents throughout the whole molecules (Figure 4), with slight enhancement in the ***a*** rings. The ACID plots of **B1**(T_1) and **C1**(T_1) show diamagnetic ring-currents along the perimeters and only weak diamagnetic ring-currents inside the central COT and PEN units. The FLU index points out that the global π-delocalization through the perimeter is similarly effective in **A1**(T_1), **B1**(T_1), and **C1**(T_1) because the $FLU_{bab'}$

Table 3. FLU and γ_x Values Computed for All the Possible (Local, Semi-Global, and Global) Circuits in S_0 and T_1 States for A3LL and *cis*-A3BB

compound	electronic state	circuit along perimeter of ring(s)	FLU	γ_x
A3LL	S_0	***a***	0.0490	
		b	0.0182	
		c	0.0059	
		a + ***b***	0.0292	
		b + ***c***	0.0114	
		b + ***a*** + ***b′***	0.0227	
		c + ***b*** + ***a*** + ***b′*** + ***c′***	0.0141	
	T_1	***a***	0.0384	0.3464
		b	0.0173	0.4138
		c	0.0077	1.7904
		a + ***b***	0.0198	0.0015
		b + ***c***	0.0090	0.7286
		b + ***a*** + ***b′***	0.0135	0.3333
		c + ***b*** + ***a*** + ***b′*** + ***c′***	0.0068	0.0624
***cis*-A3BB**	S_0	***a***	0.0435	
		b	0.0070	
		c	0.0144	
		a + ***b***	0.0257	
		b + ***c***	0.0071	
		b + ***a*** + ***b′***	0.0198	
		c + ***b*** + ***a*** + ***b′*** + ***c′***	0.0148	
	T_1	***a***	0.0345	0.3660
		b	0.0190	0.3088
		c	0.0044	0.1213
		a + ***b***	0.0191	0.4442
		b + ***c***	0.0104	0.3513
		b + ***a*** + ***b′***	0.0139	0.5088
		c + ***b*** + ***a*** + ***b′*** + ***c′***	0.0073	0.5970

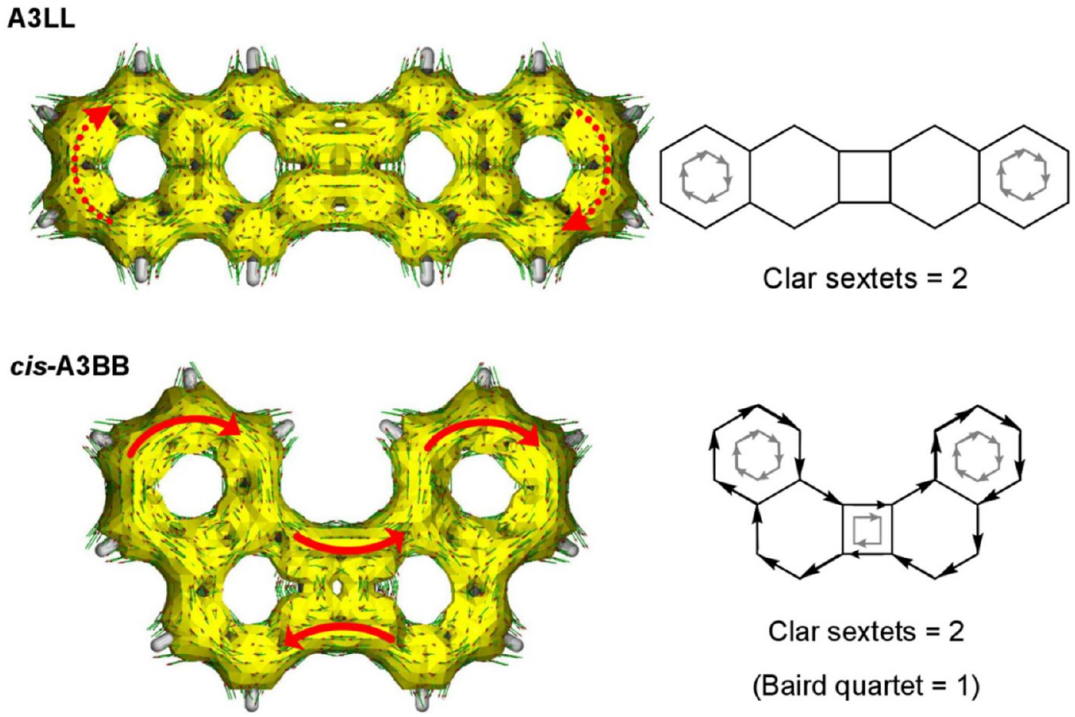

Figure 9. ACID plots of **A3LL** and *cis*-**A3BB** in their T_1 states and schematic drawings of the ring-currents. Black arrows represent stronger currents while gray arrows represent weaker currents.

DOI: 10.1021/acs.joc.7b00906
J. Org. Chem. 2017, 82, 6327−6340

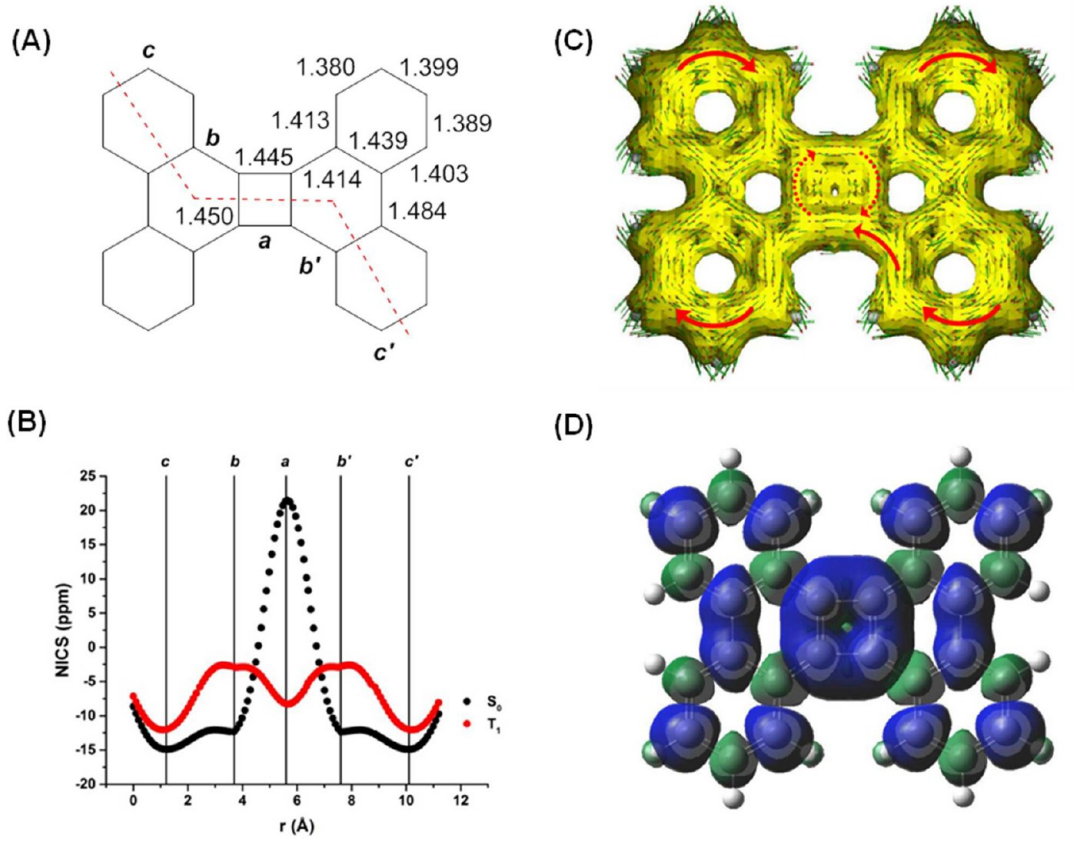

Figure 10. (A) Bond lengths and naming of rings, (B) NICS-*XY*-scans in the S_0 and T_1 states, (C) ACID plot in the T_1 state, (D) T_1 state spin density map (isosurface value, 0.0004) of **A4BBBB** calculated at the (U)B3LYP/6-311+G(d,p) level.

values are 0.0082, 0.0085, and 0.0066, respectively (Table 1 and Table S3). However, the γ values show important differences between **A1** and **C1**, on one side, and **B1** on the other. While **A1**(T_1) and **C1**(T_1) have Baird-aromatic characters in the perimeters ($\gamma_{bab'}$(**A1**) = 1.00, $\gamma_{bab'}$(**C1**) = 0.61), this is not the case for **B1**(T_1) ($\gamma_{bab'}$ = 0.01). Accordingly, **B1**(T_1) seems better represented by two Hückel-aromatic π-sextets in the ***b*** rings (FLU_b = 0.0150, γ_b = 0.06) and a Baird-aromatic ***a*** ring (FLU_a = 0.0098, γ_a = 0.58). This is also in agreement with the spin density distribution, which for **A1**(T_1) and **C1**(T_1) has a larger distribution onto the ***b*** rings than what is the case in **B1**(T_1) (see Figures S93 and S100 spin density distributions). HOMA to some extent supports the view from FLU because the ***a*** ring in **B1**(T_1) has a higher positive value than in **A1**(T_1) and **C1**(T_1), and **B1**(T_1) has the smallest HOMA value for the perimeter. The shift in aromaticity when going from **C1**(S_0) to **C1**(T_1) is clear from HOMA because the value for the ***b*** rings decreases by 0.310 while it increases by 0.424 for central PEN unit. Simultaneously, the HOMA(peri) increases to 0.858, suggesting that **C1**(T_1) primarily has a global aromaticity along the perimeter.

In conclusion, all three species **A1**−**C1** are influenced by Hückel-aromaticity in S_0 and by Baird-aromaticity in T_1 and can accordingly be labeled as aromatic chameleons. Now, having identified the tendency of these compounds to redistribute their electron density when going from S_0 to T_1, and to act as aromatic chameleons, how does this change upon benzannelation? Such additional benzannelation may impede the ability of the electronic structure readjustment in the T_1 state, but it may also depend on the connectivity (*vide infra*), and on the size of the central $4n\pi$-electron unit. An effect on the connectivity is indeed observed in the relaxed T_1 state energies as seen next.

T_1 Energies and HOMO−LUMO Energy Gaps. When going from linear to bent connectivities within a group of isomeric **A3**, **B3**, and **C3** compounds, the $E(T_1)$ energies in general decrease (Table 2 and Figure 6A). Among these three isomer classes, the **A3** isomers show the largest variation while the **B3** isomers show the smallest. Noteworthy, no significant differences in $E(T_1)$ between cis and trans configurations are observed; for **A3** and **C3**, the cis- and trans-isomers have similar $E(T_1)$ while it is 0.08 eV lower for *cis*-**B3BB** than for *trans*-**B3BB**.

When going from **A1** and **C1** to **A4BBBB** and **C4BBBB**, respectively, one sees that the $E(T_1)$ of classes **A** and **C** decrease successively, approaching those of CBD (0.23 eV) and PEN (0.34 eV), respectively. Yet, for class **B** such a gradual decrease is not observed as the $E(T_1)$ of **B4BBBB** is far from that of COT (0.67 eV). The reason is likely that **B4BBBB**(T_1) is unable to attain a planar conformation due to gradually larger steric congestion between the H atoms of the central COT ring and those at the four outer benzene rings when approaching planarity. Indeed, the $E(T_1)$ of **B4BBBB** is even larger than those of the two **B3BB** isomers.

A further interesting finding is that $E(T_1)$ for the linear compounds within class A for the shortest few members go up; for **A1**, **A2L**, and **A3LL**, the $E(T_1)$ increases from 1.92 eV to 2.22 and 2.75 eV, respectively, while for **A4LLLL** it is lowered to 1.70 eV. This initial increase in $E(T_1)$ followed by a decrease is difficult to rationalize as there is no dominating factor

DOI: 10.1021/acs.joc.7b00906
J. Org. Chem. 2017, 82, 6327−6340

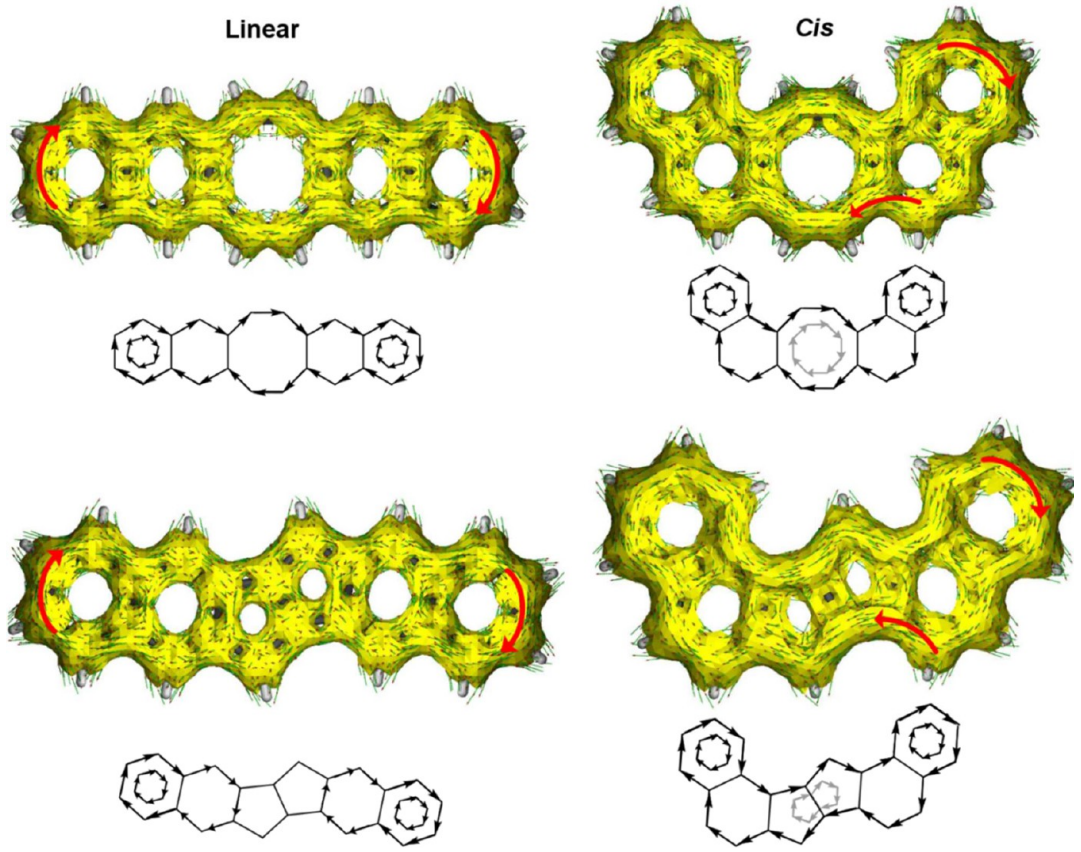

Figure 11. ACID plots for the linear and cis isomers of class **B3** and **C3** compounds in their T_1 states and schematic drawings of the ring-currents.

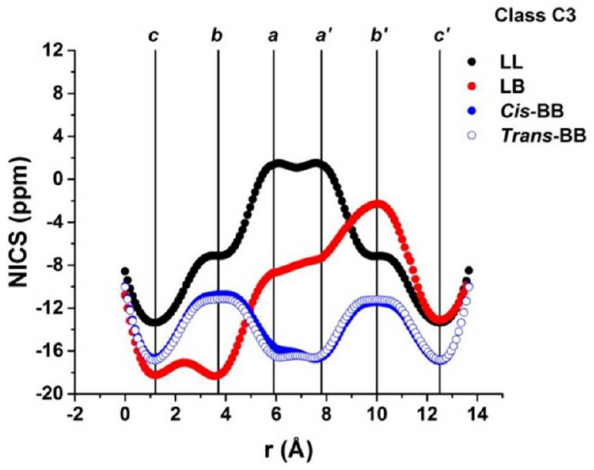

Figure 12. NICS-*XY*-scans of the **C3** isomers in the T_1 state at the UB3LYP/6-311+G(d,p) level.

stabilizing the S_0 state for the shorter compounds and destabilizing this state for the **A4LLLL** or alternatively influencing the T_1 state in the opposite sense. The variations in the $E(T_1)$ for the **A1**, **A2L**, **A3LL**, and **A4LLLL** is rather the results of a series of counteracting effects (see section 2 in the Supporting Information). One sees a tendency for a similar increase in class B as $E(T_1)$ goes up by 0.66 eV when going from **B1** to **B2L** but it then decreases for **B3LL**. However, for class C the linear compounds ranging from **C1** to **C4LLLL** have $E(T_1)$ within 1.30−1.43 eV.

The $\Delta\varepsilon_{HOMO-LUMO}$ of classes **A3** and **C3** (Figure 6B) show similar trends from the connectivity as the $E(T_1)$. Since the $\Delta\varepsilon_{HOMO-LUMO}$ are obtained for the S_0 state, at the corresponding optimal geometries, the reason for the lack of dependence of $\Delta\varepsilon_{HOMO-LUMO}$ on connectivity in **B3** is the marked nonplanarity of these systems in the S_0 states which result in weaker conjugation. Now, how do the variations in $E(T_1)$ among different isomers link with the connectivity and aromaticity? And how does it influence even larger benzannelated class A compounds?

Class A Compounds. If there is a variation in the $E(T_1)$ due to the connectivity, it should be visible in the relative isomer energies in the T_1 state. Moreover, our hypothesis is that an isomer which hosts a larger number of aromatic cycles, regardless if closed-shell Clar π-sextets or triplet diradical Baird π-quartets or π-octets, should have a lower relative energy than an isomer with a smaller number of such units. Thus, we probe if Clar's rule can be extended to involve also $4n\pi$-electron circuits that are Baird-aromatic, and we first test the hypothesis on class A and subsequently on classes B and C. Will the correctness of the hypothesis and its applicability depend on the size of the ***a*** ring?

In the S_0 state the *cis*- and *trans*-**A3BB** isomers are 12.5 kcal/mol (~0.54 eV) higher in energy than **A3LL** (Figure 7). On the other hand, in the T_1 state it is the opposite because now the two **A3BB** isomers are 26.8−26.9 kcal/mol (~1.2 eV) more stable than **A3LL**, a finding that resembles the situation between phenanthrene and anthracene in their S_0 states as well as that between various heptabenzenoid isomers (*vide supra*).[27] Noteworthy, the closest H···H distances in *cis*-**A3BB** in the S_0 and T_1 states are 2.227 and 2.213 Å, respectively, and the

DOI: 10.1021/acs.joc.7b00906
J. Org. Chem. 2017, 82, 6327−6340

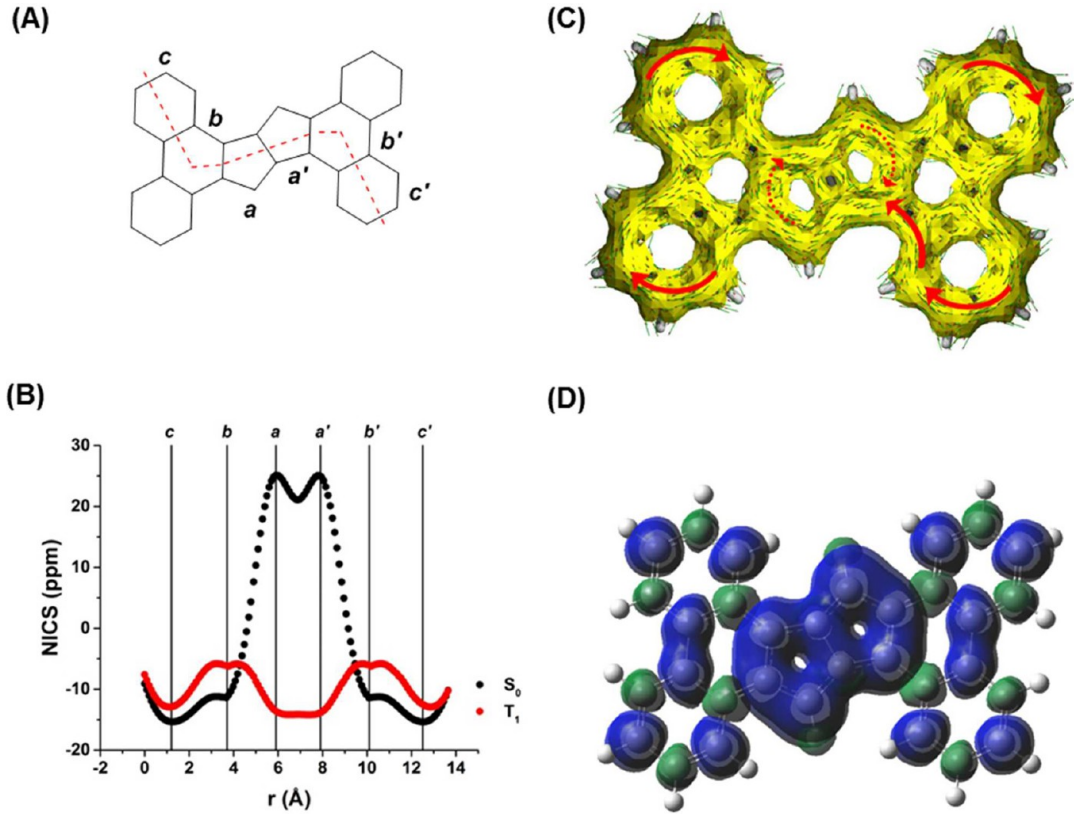

Figure 13. (A) Direction of NICS-*XY*-scan and naming of rings, (B) NICS-*XY*-scans, (C) ACID plot (T_1 state), and (D) spin density (isosurface value, 0.0004) for **C4BBBB** at the (U)B3LYP/6-311+G(d,p) level.

compound is planar in both states, indicating that differences in relative isomer energies are not caused by nonbonded H···H repulsions in the S_0 state.

As seen in Table 2, the decrease in $E(T_1)$ when going from **A3LL** to *cis*- and *trans*-**A3BB** is ∼1.7 eV (∼39 kcal/mol), and Figure 7 thus shows that this decrease to 69% is due to thermodynamic stabilization in the T_1 state and to 31% due to destabilization in the S_0 state. Interestingly, the energy difference between **A3LL**(T_1) and **A3BB**(T_1) is more than twice that between pentacene and picene in their S_0 states (15.6 kcal/mol in favor of picene), where picene hosts three π-sextets while pentacene only hosts one. So what can be the cause for the large stabilization of **A3BB**(T_1) when compared to **A3LL**(T_1)?

In the S_0 states of the **A3** isomers, the shapes of the NICS-*XY*-scans show more diatropic ring-currents for rings ***c*** than rings ***b*** while there is a local paratropic current for the central CBD unit (ring ***a***) (see Figures S13 and S15). Moreover, when going from the linear connectivity in **A3LL**(S_0) to the bent connectivity in **A3BB**(S_0), the central ***a*** ring exhibits an increase in the $NICS_{(1.7)\pi zz}$ value from 4.6 to 17.3 ppm. This is supported by the ACID results (Figure 9) as well as by the HOMA values which for the ***a*** ring goes from −0.821 in **A3LL**(S_0) to −1.256 in *cis*-**A3BB**(S_0). Hence, when going from the linear to the bent connectivities ring ***a*** becomes more antiaromatic, in line with the increase in relative S_0 isomer energies (Figure 7).

However, more significant changes are observed for the four isomers in their T_1 states. For **A3LL**(T_1) a weak diatropic current is found for the outer benzene rings (rings ***c*** and ***c***′, Figure 8), while weak paratropic ring-currents exist for rings ***b*** and ***a***. When going to **A3LB**(T_1), a significant change in rings ***c***, ***b***, and ***a*** is observed as all three gain diatropicity (Figure 8). The ring ***c***′ (right side in plot) shows slight decrease and ring ***b***′ is not affected at all in comparison to **A3LL**(T_1) because the $NICS_{(1.7)\pi zz}$ value of ring ***c***′ is decreased. Continuing to *cis*-**A3BB**(T_1) and *trans*-**A3BB**(T_1), the $NICS_{(1.7)\pi zz}$ values of all rings drop significantly in comparison to **A3LL**(T_1). The NICS-*XY*-scans in particular suggest the two fully bent isomers have three local aromatic rings (the ***a*** ring and the two ***c*** and ***c***′ rings). The ***a*** rings in the *cis*- and *trans*-**A3BB** isomers show $NICS_{(1.7)\pi zz}$ values (−12.3 ppm for *cis*-**A3BB** and −12.6 ppm for *trans*-**A3BB**) which are similar to that of CBD in the T_1 state (−12.7 ppm, see the Supporting Information). With regard to the ***c*** rings in the two **A3BB** isomers they have $NICS_{(1.7)\pi zz}$ values (−15.2 and −15.0 ppm) which are quite close to that of benzene in its S_0 state (−17.6 ppm). Additionally, there is a perimetric 20π-electron diatropic current.

The ACID plot of the T_1 state of **A3LL**(T_1) shows very weak diatropic ring-currents in the outer ***c*** and ***c***′ rings while the inner biphenylene unit displays no current (Figure 9). Conversely, when going to *cis*-**A3BB**(T_1), a clear diatropic ring-current along the 20π-electron perimeter and weak local diatropic ring-currents inside the ***c*** and ***a*** rings are observed, representing two Hückel-aromatic π-sextets (***c*** rings) and one triplet biradical Baird-aromatic π-quartet (ring ***a***). In terms of FLU, similar values are observed for **A3LL** and *cis*-**A3BB** in their T_1 states. In both cases, the outer benzene ring (FLU_c = 0.0077/0.0044), the naphthalene unit (FLU_{bc} = 0.009/0.0104), and the whole perimeter ($FLU_{cbab'c'}$ = 0.0068/0.0073) are the most efficient circuits for π-delocalization (Table 3). However,

DOI: 10.1021/acs.joc.7b00906
J. Org. Chem. 2017, 82, 6327−6340

Table 4. FLU and γ_x Values Computed for All the Possible (Local, Semi-Global, and Global) Circuits in S_0 and T_1 States for A4BBBB, B4BBBB, and C4BBBB

compound	electronic state	circuit along perimeter of ring(s)	FLU	γ_x
A4BBBB	S_0	*a*	0.0434	
		b	0.0131	
		c	0.0077	
		a + *b*	0.0315	
		a + *b* + *c*	0.0296	
		b + *c*	0.0091	
		c + *b* + *c*	0.0073	
		b + *a* + *b*′	0.0220	
		c + *b* + *a* + *b*′ + *c*′	0.0177	
		perimeter	0.0135	
	T_1	*a*	0.0307	0.4631
		b	0.0241	0.2473
		c	0.0043	0.1172
		a + *b*	0.0234	0.3941
		a + *b* + *c*	0.0210	0.3605
		b + *c*	0.0141	0.2562
		c + *b* + *c*	0.0098	0.2656
		b + *a* + *b*′	0.0152	0.4043
		c + *b* + *a* + *b*′ + *c*′	0.0122	0.3746
		perimeter	0.0084	0.3897
B4BBBB	S_0	*a*	0.0487	
		b	0.0209	
		c	0.0050	
		a + *b*	0.0425	
		a + *b* + *c*	0.0324	
		b + *c*	0.0134	
		c + *b* + *c*	0.0102	
		b + *a* + *b*′	0.0393	
		c + *b* + *a* + *b*′ + *c*′	0.0269	
		perimeter	0.0208	
	T_1	*a*	0.0082	0.7583
		b	0.0250	0.1600
		c	0.0031	0.1180
		a + *b*	0.0152	0.2752
		a + *b* + *c*	0.0116	0.2781
		b + *c*	0.0153	0.1656
		c + *b* + *c*	0.0111	0.1710
		b + *a* + *b*′	0.0188	0.1702
		c + *b* + *a* + *b*′ + *c*′	0.0127	0.1756
		perimeter	0.0097	0.1808
C4BBBB	S_0	*a* + *a*′	0.0326	
		b	0.0154	
		c	0.0059	
		a + *a*′ + *b*′	0.0294	
		b + *c*	0.0102	
		c + *b* + *c*	0.0080	
		c + *b* + *a* + *a*′ + *b*′ + *c*′	0.0194	
		b + *a* + *a*′ + *b*′	0.5858	
		perimeter	0.0152	
	T_1	*a* + *a*′	0.0119	0.7945
		b	0.0233	0.2657
		c	0.0036	0.0611
		a + *a*′ + *b*′	0.0151	0.3697
		b + *c*	0.0142	0.2432
		c + *b* + *c*	0.0102	0.2368
		c + *b* + *a* + *a*′ + *b*′ + *c*′	0.0113	0.2038
		b + *a* + *a*′ + *b*′	0.0167	0.2186
		perimeter	0.0085	0.1893

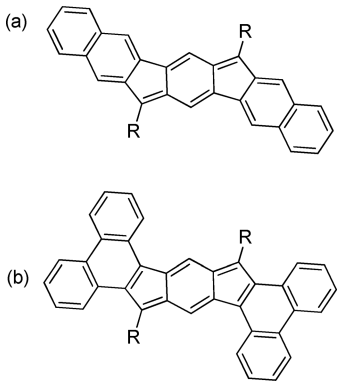

Figure 14. Structures of (a) dinaphthoindacene and (b) diphenanthrenoindacene.

there are important differences according to γ. Thus, **A3LL** presents a high Baird-aromatic character in the outer benzene ring (γ_c = 1.79) and a Hückel-aromatic character in the perimeter ($\gamma_{cbab'c'}$ = 0.06), whereas the outer benzene ring in *cis*-**A3BB** is basically Hückel aromatic (γ_c = 0.12) and the perimeter is Baird aromatic ($\gamma_{cbab'c'}$ = 0.60). The results of FLU suggests presence of two Clar π-sextets and one Baird π-octet around the phenylene in *cis*-**A3BB**(T_1) similar to the **A2B**(T_1). The ACID plot of **A2B**(T_1) clearly shows one Baird π-octet and one Clar π-sextet (see Figure S25). However, the ACID plot of *cis*-**A3BB**(T_1) does not support the presence of a Baird π-octet because the ring-current of the Baird π-octet is counteracted upon by the two adjacent Clar π-sextets.

With regard to HOMA, one can see that the degree of aromaticity in the ***c*** rings in the two **A3BB**(T_1) isomers, and in the bent segment of **A3LB**(T_1) increases when compared to that of the ***c*** rings of **A3LL**(T_1). Thus, Hückel-aromatic π-sextets form in the bent segments. However, the HOMA values of the ***a*** rings in the T_1 state **A3** isomers (except **A3LB**) represent nonaromatic situations, in line with the low HOMA for CBD in the T_1 state, corresponding to only a very weak Baird-aromaticity.[S1] Interestingly, the HOMA(peri) has values within 0.75−0.80, suggesting global perimetric T_1 aromaticity of similar strengths in all the four isomers.

So what is the reason for the T_1 state stabilization found in **A3BB**? The four different methods of aromaticity determination clearly give different answers, and it is not obvious that our working hypothesis on usage of Baird's rule in a Clar's rule context is useful for the rationalization of the $E(T_1)$ of the **A3** isomers.

In this context, one can regard **A4BBBB** (Figure 10), a compound which could exhibit a particularly pronounced T_1 state stabilization and aromaticity since it is analogous to tetrabenzanthracene, i.e., the fully benzenoid isomer among the heptabenzenoid PAHs. Compound **A4BBBB** has an $E(T_1)$ of 0.62 eV (Table 1), i.e., 1.08 eV lower than that of **A4LLLL**. Indeed, the NICS-*XY*-scan and the ACID plot reveal a global current along the perimeter and, additionally, localized currents in the π-sextets of the ***c*** rings as well as the π-quartet of the ***a***

DOI: 10.1021/acs.joc.7b00906
J. Org. Chem. 2017, 82, 6327−6340

ring (Figure 10). This gives support for the interpretation that **A4BBBB**(T_1) to some extent has four Hückel-aromatic π-sextets and one Baird-aromatic π-quartet. The view is in line with the calculated spin density as the spin is mostly localized to the central CBD unit (Figure 10D). However, FLU gives a different description as it indicates local Hückel-aromaticity in the ***c*** rings (FLU_c = 0.0043, γ_c = 0.12) as well as semiglobal ($FLU_{cbc'}$ = 0.0098, $\gamma_{cbc'}$ = 0.27) and global ($FLU_{perimeter}$ = 0.0083, $\gamma_{perimeter}$ = 0.39) circuits efficient for π-delocalization. According to FLU, the perimeter has the highest Baird-aromatic character. Finally, the HOMA values in the T_1 state suggest strong aromaticity in the ***c*** rings (0.844) and reasonably strong along the perimeter (0.708). In contrast, the ***a*** ring is nonaromatic (0.082) according to HOMA and this also applies to the ***b*** rings (0.155). Yet, the situation resembles that of T_1 state CBD, which was considered based on HOMA to have weaker T_1 aromaticity.[51]

Class B and C Compounds. Since it is known that CBD displays a lower extent of T_1 state aromaticity than larger [4*n*]annulenes,[51−53] our hypothesis may work better in classes B and C with central 8π-electron units. The triplet energies of **B2** and **C2** series are also affected upon bending. There is a significant difference in $E(T_1)$ between **B2L** and **B2B** (0.73 eV), but as one goes to the **B3** isomers one finds that $E(T_1)$ only depends weakly on connectivity (Table 2 and Figure 6A). Moreover, for $\Delta\varepsilon_{HOMO-LUMO}$ there is no variation among the **B3** isomers (Figure 6B), the latter an effect of the puckering of the COT ring in the S_0 states. Conversely, the difference in $E(T_1)$ between **C2L** and **C2B** is smaller (0.40 eV) than between **B2L** and **B2B**, yet in the **C3** isomers, the 8π-electron PEN unit is planar and the effects of connectivity on both $E(T_1)$ and $\Delta\varepsilon_{HOMO-LUMO}$ are clear.

Increasing the benzannelation around the COT unit in the class B compounds gradually makes them nonplanar also in their T_1 states, a feature that results from steric congestion between nonbonded H atoms. Because of the nonplanarity the NICS-*XY*-scans show discontinuities both in *trans*-**B3BB** and *cis*-**B3BB** (see the Figure S14), resembling a finding by Schaffroth et al., who reported discontinuous NICS-*XY*-scans arising from nonplanarity of adjacent six- and four-membered rings in tetraazaacenes.[55] Moreover, the ACID plot of **B3LL**(T_1) exhibits diamagnetic ring-currents going along the perimeter of the whole molecule (Figure 11). The ACID plots of *cis*/*trans*-**B3BB**(T_1) show similar magnetic properties as *cis*/*trans*-**A3BB**(T_1) with several different ring-currents; one that moves along the perimeter but also local diamagnetic ring-currents inside the ***c*** and ***a*** rings.

The **B3** and **C3** isomers with bent connectivities are 17.0 and 7.3 kcal/mol more stable in their T_1 states than the corresponding linear isomers (see the Supporting Information), which is smaller than found for the **A3** isomers (*vide supra*). However, these gains are now more clearly consequences of the existence of three local aromatic cycles in the bent isomers; two Clar π-sextets in the ***c*** rings and one Baird-aromatic π-octet. Yet, the reason for the smaller gains in energy in T_1 when going from **3LL** to **3BB** isomers for class B and C than for class A seems connected to the varying gains of closed-shell Hückel-aromaticity in the ***c*** rings in the different compound classes. When going from **A3LL** to **A3LB** there is a significant lowering in the $NICS_{(1.7)\pi zz}$ from −3.1 to −15.3 ppm, but when going from **C3LL** to **C3LB** the lowering is more modest from −13.4 to −16.9 ppm in rings ***c*** (see Figure S15). In the S_0 state, the relative isomer energies when going from the fully linear **3LL** isomers to the doubly bent **3BB** increase by 0.9 and 7.8 kcal/mol in the **B3** and **C3** classes, respectively (see Figure S5).

For the class **C3** isomers, similar as for class **A3** isomers, the NICS-*XY*-scan in the T_1 states show an overall increase in the aromaticity when going from linear to cis/trans connectivity, and this is the case for both the ***c*** and ***c′*** rings and the central ***aa′*** (PEN) moiety (Figure 12). Interestingly, the two ***c*** rings in **C3LL** are significantly more aromatic according to NICS-*XY*-scans than the corresponding rings in **A3LL** (see Figure S15). The ACID plots in the T_1 state display diatropic ring-currents in all **C3** compounds, yet a weak ring-current in the central pentalene is found in *cis*- and *trans*-**C3BB** (Figure 11).

With regard to **C4BBBB** it is, in contrast to **B4BBBB**, completely planar in both its S_0 and T_1 states (see Figures S80 and S82). The fully benzannelated **C4BBBB**(T_1) (Figure 13) shows similar properties as **A4BBBB**(T_1), but it is particularly noteworthy that the most diamagnetic units in the T_1 state are the ***a*** rings according to NICS-*XY*-scan. Hence, it has five aromatic cycles, four disjointed closed-shell Clar π-sextets and one disjointed triplet biradical Baird π-octet.

The ACID plot in the T_1 state reveals diamagnetic ring-currents along the 32π-electron perimeter along with some diamagnetic ring-currents in the benzene rings and the central pentalene unit. Similar as for **A4BBBB**(T_1), the spin-densities of **B4BBBB**(T_1) and **C4BBBB**(T_1) are mostly localized to the central 8π-electron moieties (see Figure S99 and Figure 13D, respectively).

In terms of FLU (Table 4), **C4BBBB**(T_1) shows similar properties as **A4BBBB**(T_1). Specifically, the highest localization is found in the inner benzene ring (FLU_b = 0.0233−0.0241) while the two outer benzene rings (FLU_c = 0.0036−0.0043) are more Hückel-aromatic. The phenanthrene moiety has also two semiglobal circuits, the naphthalene unit (***bc***) and the phenanthrene unit (***cbc***). The latter (FLU_{cbc} = 0.0098−0.0102) is more delocalized than the former (FLU_{bc} = 0.0142−0.0141). Yet, the most efficient circuit for π-delocalization is the perimeter ($FLU_{perimeter}$ = 0.0084−0.0085) which has Hückel-aromatic character according to the γ value. Noteworthy, the pentalene unit in **C4BBBB**(T_1) is more Baird aromatic than the 4-MR in **A4BBBB**(T_1) ($FLU_{aa'}$ = 0.0119 and $\gamma_{aa'}$ = 0.7945 vs FLU_a = 0.0307 and γ_a = 0.4631, respectively). With regard to the **B4BBBB**(T_1) it is best described as four Clar π-sextets in the outer 6-MRs (FLU_c = 0.0031) and one Baird π-octet in the 8-MR (FLU_a = 0.0082 and γ_a = 0.7583).

The HOMA values of **B4BBBB**(T_1) indicate four Clar π-sextets (0.904), one Baird π-octet (0.734), and a somewhat weaker aromaticity along the perimeter (0.632). In comparison, for **C4BBBB**(T_1), the HOMA values show four Clar π-sextets (0.882), a weaker Baird π-octet in the central PEN unit (0.667), and a somewhat stronger aromaticity along the perimeter (0.747). The CC bonds of the ***b*** rings in both **B4BBBB**(T_1) and **C4BBBB**(T_1) have bond lengths that are relatively long (longer than the corresponding bonds in **A4BBBB**(T_1)) and they have more single bond character, in agreement with nonaromatic HOMA values of 0.032 and 0.246 for the ***b*** rings of **B4BBBB**(T_1) and **C4BBBB**(T_1), respectively.

Previous Experimental Findings on Analogous Compounds. Some of the compounds which we discuss in our study were previously synthesized and they showed interesting electronic properties. When going from the linear to the cis- and trans-connectivities in dinaphthoindacene isomers (Figure 14), red-shifted absorptions in the UV−vis spectra are observed. This is in agreement with our observation that cis/

DOI: 10.1021/acs.joc.7b00906
J. Org. Chem. 2017, 82, 6327−6340

trans connectivity has significant influence on the triplet energies. It is reported that the double bond character of the fused CC bond between the arene and the central indacene/pentalene unit is important in controlling the antiaromaticity of the central unit.[24,56] Above we show that the magnetic properties (NICS scans and ACID plots) of central 4*n* rings are changed drastically when going from S_0 to the T_1 states as an influence of T_1 aromaticity. However, the antiaromaticity of the pentalene core can be tuned by changing the degree of aromaticity of the peripheral rings attached to the pentalene unit.[57]

Moreover, red-shifts in the UV−vis spectra of Class **A3** compounds were also observed when going from the linear to the cis/trans bent connectivities.[58−60] While Cava and co-workers and Barton separately reported that the cis/trans isomers of Class **A3** compounds are only stable in the dark,[61,62] a later study by Lohman showed that the *cis*/*trans*-**A3** compounds are photostable.[63] The light sensitivity of class **A3** compounds can tentatively be related to lower T_1 aromaticity of the cyclobutadiene as a central unit.

The electronic properties of class B compounds, **B1**, **B3LL**, and **B4LLLL** are enhanced upon increased conjugation, and they are reported to have interesting applications as photo-responsive columnar liquid crystal materials.[64]Among the **C3** isomers, **C3LL** and *cis*- as well as *trans*-**C3BB** are synthesized previously and **C3LL** could be useful for organic heterojunction photovoltaic cells.[65]

Finally, it is argued that a conjugated polyaromatic hydrocarbon is stable toward oxidation if $E(T_1)$ of the polyaromatic hydrocarbon is smaller than the $E(T_1)$ of oxygen.[66] In all three series of compounds, the $E(T_1)$ are decreasing as a function of connectivity, which should lead to a gain in stability.

CONCLUSIONS

Our present study illustrates the use of Baird's rule as a back-of-an-envelope tool for rationalization of excited state properties of π-conjugated hydrocarbons and, ultimately, for the design of molecules with targeted optical properties. We also show that Clar's rule, if connected to Baird's rule, can be extended to the T_1 state of fully benzenoid hydrocarbons provided that a central benzene unit is replaced by either a 4π-electron CBD ring or an 8π-electron COT or PEN unit. In the T_1 states, these units take the character of local triplet state Baird-aromatic units, leaving the other rings relatively undisturbed. The optoelectronic properties of π-conjugated hydrocarbons can therefore be modulated by the insertion of 4*n*π-electron antiaromatic units. When comparing several different isomeric compounds having a central 4*n*π-electron unit, the isomer that is most stable is the one that allows for the largest number of Clar π-sextets and Baird π-quartet/octets combined. The lowest triplet energy is observed for the **C4BBBB** isomer containing five aromatic cycles, four disjointed Clar π-sextets, and one disjointed Baird π-octet. Thus, using Baird's rule on triplet state (anti)-aromaticity together with Clar's rule, one can rationalize the triplet state energies of a range of compounds with potential applicability in organic electronics.

ASSOCIATED CONTENT

Supporting Information

The Supporting Information is available free of charge on the ACS Publications website at DOI: 10.1021/acs.joc.7b00906.

Orbital energies, FLU values, ACID plots, NICS-*XY* scans, NICS-scans of **B1**, HOMA values, spin densities, and Cartesian coordinates (PDF)

AUTHOR INFORMATION

Corresponding Authors

*E-mail: henrik.ottosson@kemi.uu.se.
*E-mail: miquel.sola@udg.edu.

ORCID

Miquel Solà: 0000-0002-1917-7450
Henrik Ottosson: 0000-0001-8076-1165

Notes

The authors declare no competing financial interest.

ACKNOWLEDGMENTS

The Erasmus Mundus EXPERTS III is acknowledged for a Ph.D. scholarship to R.A., and the Swedish Research Council (Vetenskapsrådet) is acknowledged for financial support. The Swedish Infrastructure for Computing (SNIC) at NSC and UPPMAX (Grants SNIC-2016-1-74 and SNIC-2016/7-21) are greatly acknowledged for the generous allotment of computer time. M.S. and O.E.B. acknowledge the Ministerio de Economía y Competitividad (MINECO) of Spain (Project CTQ2014-54306-P), the Generalitat de Catalunya (Project 2014SGR931, Xarxa de Referència en Química Teòrica i Computacional, ICREA Academia 2014 Prize for M.S. and Grant No. 2014FI_B 00429 to O.E.B.), and the EU under the FEDER Grant UNGI10-4E-801 (European Fund for Regional Development).

REFERENCES

(1) (a) Denis, P. A. *J. Phys. Chem. C* **2014**, *118*, 24976. (b) Parkhurst, R. R.; Swager, T. M. *J. Am. Chem. Soc.* **2012**, *134*, 15351. (c) Miljanić, O. Š.; Vollhardt, K. P. C. *Carbon-Rich Compounds: From Molecules to Materials*; Haley, M. M., Tykwinsky, R. R., Eds.; Wiley-VCH: Weinheim, Germany, 2006; p 140. (d) Ooi, T.; Takahashi, M.; Maruoka, K. *J. Am. Chem. Soc.* **1996**, *118*, 11307. (e) Kwong, C.-Y.; Leung, M.-K.; Lin, S.-C.; Chan, T.-L.; Chow, H.-F. *Tetrahedron Lett.* **1996**, *37*, 5913. (f) Mindach, L.; Müllen, K. *Adv. Mater.* **1996**, *8*, 504. (g) Vollhardt, K. P. C. *Pure Appl. Chem.* **1993**, *65*, 153. (h) Kelly, T. R.; Meghani, P.; Ekkundi, V. S. *Tetrahedron Lett.* **1990**, *31*, 3381. (i) Chang, C. K.; Abdalmuhdi, I. *Angew. Chem., Int. Ed. Engl.* **1984**, *23*, 164.

(2) (a) Fukazawa, A.; Oshima, H.; Shimizu, S.; Kobayashi, N.; Yamaguchi, S. *J. Am. Chem. Soc.* **2014**, *136*, 8738. (b) Yuan, C.; Saito, S.; Camacho, C.; Kowalczyk, T.; Irle, S.; Yamaguchi, S. *Chem. - Eur. J.* **2014**, *20*, 2193.

(3) Schneebeli, S.; Kamenetska, M.; Foss, F.; Vazquez, H.; Skouta, R.; Hybertsen, M.; Venkataraman, L.; Breslow, R. *Org. Lett.* **2010**, *12*, 4114.

(4) Gershoni-Poranne, R.; Gibson, C. M.; Fowler, P. W.; Stanger, A. *J. Org. Chem.* **2013**, *78*, 7544.

(5) Radenković, S.; Tošović, J.; Havenith, R. W. A.; Bultinck, P. *ChemPhysChem* **2015**, *16*, 216.

(6) (a) Maksic, Z. B.; Kovaček, D.; Eckert-Maksić, M.; Böckmann, M.; Klessinger, M. *J. Phys. Chem.* **1995**, *99*, 6410. (b) Schulman, J. M.; Disch, R. L. *J. Am. Chem. Soc.* **1996**, *118*, 8470. (c) Parkhurst, R. R.; Swager, T. M. Antiaromaticity in Nonbenzenoid Oligoarenes and Ladder Polymers. In *Polyarene II*; Topics in Current Chemistry, Vol. *350*; Seigel, J. S., Wu, Y.-T., Eds.; Springer-Verlag: Berlin, Heidelberg, Germany, 2014; p 141.

(7) Dosche, C.; Löhmannsröben, H.-G.; Bieser, A.; Dosa, P. I.; Han, S.; Iwamoto, M.; Schleifenbaum, A.; Vollhardt, K. P. C. *Phys. Chem. Chem. Phys.* **2002**, *4*, 2156.

(8) El-Bakouri, O.; Poater, J.; Feixas, F.; Solà, M. *Theor. Chem. Acc.* **2016**, *135*, 205.

DOI: 10.1021/acs.joc.7b00906
J. Org. Chem. 2017, 82, 6327−6340

(9) Randić, M. *J. Am. Chem. Soc.* **1977**, *99*, 444.
(10) (a) Dietz, F.; Tyutyulkov, N.; Rabinovitz, M. *J. Chem. Soc., Perkin Trans. 2* **1993**, 157. (b) Dietz, F.; Rabinovitz, M.; Tadjer, A.; Tyutyulkov, N. *J. Chem. Soc., Perkin Trans. 2* **1995**, 735.
(11) Baird, N. C. *J. Am. Chem. Soc.* **1972**, *94*, 4941.
(12) Rosenberg, M.; Dahlstrand, C.; Kilså, K.; Ottosson, H. *Chem. Rev.* **2014**, *114*, 5379.
(13) (a) Karadakov, P. B. *J. Phys. Chem. A* **2008**, *112*, 7303. (b) Karadakov, P. B. *J. Phys. Chem. A* **2008**, *112*, 12707. (c) Karadakov, P. B.; Hearnshaw, P.; Horner, K. E. *J. Org. Chem.* **2016**, *81*, 11346.
(14) Feixas, F.; Vandenbussche, J.; Bultinck, P.; Matito, E.; Solà, M. *Phys. Chem. Chem. Phys.* **2011**, *13*, 20690.
(15) Möllerstedt, H.; Piqueras, M. C.; Crespo, R.; Ottosson, H. *J. Am. Chem. Soc.* **2004**, *126*, 13938.
(16) (a) Jorner, K.; Emanuelsson, R.; Dahlstrand, C.; Tong, H.; Denisova, A. V.; Ottosson, H. *Chem. - Eur. J.* **2014**, *20*, 9295. (b) Rosenberg, M.; Ottosson, H.; Kilså, K. *Phys. Chem. Chem. Phys.* **2011**, *13*, 12912. (c) Ottosson, H.; Kilså, K.; Chajara, K.; Piqueras, M.; Crespo, R.; Kato, H.; Muthas. *Chem. - Eur. J.* **2007**, *13*, 6998.
(17) (a) Zimmermann, R. A. *J. Mol. Struct.* **1996**, *377*, 35. (b) Bich, V. T.; Bini, R.; Salvi, P. R. *Chem. Phys. Lett.* **1990**, *175*, 413.
(18) (a) Coppo, P.; Yeates, S. G. *Adv. Mater.* **2005**, *17*, 3001. (b) Jurchescu, O. D.; Baas, J.; Palstra, T. T. M. *Appl. Phys. Lett.* **2004**, *84*, 3061.
(19) (a) Thorley, K. L.; Anthony, J. E. *Isr. J. Chem.* **2014**, *54*, 642. (b) Anthony, J. E. *Angew. Chem., Int. Ed.* **2008**, *47*, 452. (c) Anthony, J. E. *Chem. Rev.* **2006**, *106*, 5028.
(20) (a) Granger, D. B.; Mei, Y.; Thorley, K. J.; Parkin, S. R.; Jurchescu, O. D.; Anthony, J. E. *Org. Lett.* **2016**, *18*, 6050. (b) Kraft, U.; Anthony, J. E.; Ripaud, E.; Loth, M. A.; Weber, E.; Klauk, H. *Chem. Mater.* **2015**, *27*, 998. (c) Kim, C.-H.; Hlaing, H.; Payne, M. M.; Parkin, S. R.; Anthony, J. E.; Kymissis, I. *ChemPhysChem* **2015**, *16*, 1251. (d) Zhang, L.; Fonari, A.; Liu, Y.; Hoyt, A. L-M.; Lee, H.; Granger, D.; Parkin, S.; Russell, T. P.; Anthony, J. E.; Bredas, J.-L.; Coropceanu, V.; Briseno, A. L. *J. Am. Chem. Soc.* **2014**, *136*, 9248.
(21) (a) Engelhart, J. U.; Paulus, F.; Schaffroth, M.; Vasilenko, V.; Tverskoy, O.; Rominger, F.; Bunz, U. H. F. *J. Org. Chem.* **2016**, *81*, 1198. (b) Bunz, U. H. F.; Engelhart, J. U. *Chem. - Eur. J.* **2016**, *22*, 4680. (c) Hahn, S.; Biegger, P.; Bender, M.; Rominger, F.; Bunz, U. H. F. *Chem. - Eur. J.* **2016**, *22*, 869. (d) Bunz, U. H. F. *Acc. Chem. Res.* **2015**, *48*, 1676.
(22) (a) Mei, J.; Diao, Y.; Appleton, A. L.; Fang, L.; Bao, Z. *J. Am. Chem. Soc.* **2013**, *135*, 6724. (b) Yang, X.; Liu, D.; Miao, Q. *Angew. Chem., Int. Ed.* **2014**, *53*, 6786.
(23) Cao, J.; London, G.; Dumele, O.; Rekowski, M. v. W.; Trapp, N.; Ruhlmann, L.; Boudon, C.; Stanger, A.; Diederich, F. *J. Am. Chem. Soc.* **2015**, *137*, 7178.
(24) Frederickson, C. K.; Zakharov, L. N.; Haley, M. *J. Am. Chem. Soc.* **2016**, *138*, 16827.
(25) Clar, E. *The Aromatic Sextet*; Wiley: New York, 1972.
(26) Solà, M. *Front. Chem.* **2013**, *1*, 22.
(27) Poater, J.; Visser, R.; Solà, M.; Bickelhaupt, F. M. *J. Org. Chem.* **2007**, *72*, 1134.
(28) Dominikowska, J.; Palusiak, M. *Phys. Chem. Chem. Phys.* **2011**, *13*, 11976.
(29) Zhu, J.; Dahlstrand, C.; Smith, J. R.; Villaume, S.; Ottosson, H. *Symmetry* **2010**, *2*, 1653.
(30) Balaban, A. T.; Klein, D. J. *J. Phys. Chem. C* **2009**, *113*, 19123.
(31) Wu, J.; Zhu, J. *ChemPhysChem* **2015**, *16*, 3806.
(32) Frisch, M. J. et al. *Gaussian 09*, Revision D.01; Gaussian, Inc.: Wallingford CT, 2013.
(33) Stephens, P. J.; Devlin, F. J.; Chabalowski, C. F.; Frisch, M. J. *J. Phys. Chem.* **1994**, *98*, 11623.
(34) Krishnan, R.; Binkley, J. S.; Seeger, R.; Pople, J. A. *J. Chem. Phys.* **1980**, *72*, 650.
(35) Wolinski, K.; Hinton, J. F.; Pulay, P. *J. Am. Chem. Soc.* **1990**, *112*, 8251.
(36) Gershoni-Poranne, R.; Stanger, A. *Chem. - Eur. J.* **2014**, *20*, 5673.
(37) Rahalkar, A.; Stanger, A. *Aroma*. http://chemistry.technion.ac.il/members/amnon-stanger/.
(38) Stanger, A. *J. Org. Chem.* **2010**, *75*, 2281.
(39) Stanger, A. *J. Org. Chem.* **2006**, *71*, 883.
(40) (a) Herges, R.; Geuenich, D. *J. Phys. Chem. A* **2001**, *105*, 3214. (b) Geuenich, D.; Hess, K.; Kohler, F.; Herges, R. *Chem. Rev.* **2005**, *105*, 3758.
(41) Keith, T. A.; Bader, R. F. W. *Chem. Phys. Lett.* **1993**, *210*, 223.
(42) (a) Krygowski, T. M. *J. Chem. Inf. Model.* **1993**, *33*, 70. (b) Krygowski, T. M.; Szatylowicz, H.; Stasyuk, O. A.; Dominikowska, J.; Palusiak, M. *Chem. Rev.* **2014**, *114*, 6383.
(43) Matito, E.; Duran, M.; Solà, M. *J. Chem. Phys.* **2005**, *122*, 014109.
(44) Feixas, F.; Matito, E.; Poater, J.; Solà, M. *Chem. Soc. Rev.* **2015**, *44*, 6434.
(45) Fradera, X.; Austen, M. A.; Bader, R. F. W. *J. Phys. Chem. A* **1999**, *103*, 304.
(46) (a) Bader, R. F. W. *Atoms in Molecules: A Quantum Theory*; Clarendon Press: Oxford, U.K., 1990. (b) Bader, R. F. W. *Chem. Rev.* **1991**, *91*, 893.
(47) Matito, E. *ESI-3D: Electron Sharing Indexes Program for 3D Molecular Space Partitioning*. http://iqc.udg.es/~eduard/ESI, Institute of Computational Chemistry and Catalysis: Girona, Catalonia, Spain, 2014.
(48) Keith, A. *AIMAll* (v. 14.11.23); TK Gristmill Software: Overland Park KS, 2014; aim.tkgristmill.com.
(49) Jorner, K.; Feixas, F.; Ayub, R.; Lindh, R.; Solà, M.; Ottosson, H. *Chem. - Eur. J.* **2016**, *22*, 2793.
(50) (a) Beck, M. E.; Rebentisch, R.; Hohlneicher, G.; Fülscher, M. P.; Serrano-Andrés, L.; Roos, B. O. *J. Chem. Phys.* **1997**, *107*, 9464. (b) Mak, T. C. W.; Trotter, J. *J. Chem. Soc.* **1962**, 1.
(51) Krygowski, T. M.; Cyrański, M. K. *Tetrahedron* **1999**, *55*, 11143.
(52) Villaume, S.; Fogarty, H. A.; Ottosson, H. *ChemPhysChem* **2008**, *9*, 257.
(53) Taubert, S.; Sundholm, D.; Jusélius, J. *J. Chem. Phys.* **2011**, *134*, 054123.
(54) Zhu, J.; An, K.; Schleyer, P. v. R. *Org. Lett.* **2013**, *15*, 2442.
(55) Schaffroth, M.; Gershoni-Poranne, R.; Stanger, A.; Bunz, U. H. F. *J. Org. Chem.* **2014**, *79*, 11644.
(56) Kato, S-i.; Kuwako, S.; Takahashi, N.; Kijima, T.; Nakamura, Y. *J. Org. Chem.* **2016**, *81*, 7700.
(57) Oshima, H.; Fukazawa, A.; Yamaguchi, S. *Angew. Chem., Int. Ed.* **2017**, *56*, 3270.
(58) Yamaguchi, H.; Baumann, H. *J. Chem. Soc., Faraday Trans. 2* **1988**, *84*, 417.
(59) Curtis, R. F.; Viswanath, G. *J. Chem. Soc.* **1959**, 1670.
(60) Ward, E. R.; Pearson, B. D. *J. Chem. Soc.* **1959**, 1676.
(61) Cava, M. P.; Stucker, J. F. *J. Am. Chem. Soc.* **1955**, *77*, 6022.
(62) Barton, J. W. *J. Chem. Soc.* **1964**, 5161.
(63) Lohmann, J. *J. Chem. Soc., Faraday Trans. 1* **1972**, *68*, 814.
(64) (a) Saito, S.; Nobusue, S.; Tsuzaka, E.; Yuan, C.; Mori, C.; Hara, M.; Seki, T.; Camacho, C.; Irle, S.; Yamaguchi, S. *Nat. Commun.* **2016**, *7*, 12094. (b) Yuan, C.; Saito, S.; Camacho, C.; Kowalczyk, T.; Irle, S.; Yamaguchi, S. *Chem. - Eur. J.* **2014**, *20*, 2193. (c) Suzuki, S.; Maeda, S.; Morokuma, K. *J. Phys. Chem. A* **2015**, *119*, 11479.
(65) Kawase, T.; Nishida, J.-i. *Chem. Rec.* **2015**, *15*, 1045.
(66) Thomas, S.; Ly, J.; Zhang, L.; Briseno, A. L.; Bredas, J.-L. *Chem. Mater.* **2016**, *28*, 8504.

DOI: 10.1021/acs.joc.7b00906
J. Org. Chem. 2017, 82, 6327−6340